Breaking Biomphalaria black box by in situ revelation of fluorescent Schistosoma mansoni parasites

Pierre Poteaux, Chantal Ripoll, Amélie Sarrazin, Marie-Pierre Blanchard, Anne Guillou-Duvoid, Benjamin Gourbal, Hélène Hirbec, David Duval

Fish and Shellfish Immunology 153 (2024) 109800

Breaking *Biomphalaria* black box by *in situ* revelation of fluorescent *Schistosoma mansoni* parasites

Pierre Poteaux[a,*], Chantal Ripoll[b], Am´elie Sarrazin[c], Marie-Pierre Blanchard[c], Anne Guillou-Duvoid[b], Benjamin Gourbal[a], Hélène Hirbec[b], David Duval[a]

[a] *IHPE, Universié de Perpignan Via Domitia, CNRS, Ifremer, Université de Montpellier, 58 avenue Paul Alduy, 66860, Perpignan, France*

[b] *Institut de Génomique Fonctionnelle, Université de Montpellier, CNRS, INSERM, 141 rue de la Cardonille, 34091, Montpellier, France*

[c] *MRI, BioCampus Montpellier, CNRS, INSERM, Université de Montpellier, 141 rue de la Cardonille, 34091, Montpellier, France*

ABSTRACT

Tissue clearing is an old-fashioned method developed in the 1900's and used to turn an opaque biological object into a 3D visualizable transparent structure. Developed and diversified over the last decade, this method is most of the time applied to mammals' tissues, and especially mouse and human tissues for cytological, histological and pathophysiological studies. Through autofluorescence, immunofluorescence, *in situ* hybridization, intercalating agents, fluorescent transfection markers or fluorescent particle uptake, optically cleared samples can be monitored to discover new biological structures and cellular interactions through 3D-visualization, which can be more challenging in some extend through classical histological methods. Most of the tissue clearing procedures have been developed for specific applications like endogenous fluorescence visualization, immunolabeling or for revealing specific organs. Thus, choosing the adapted protocol may be empirical for non-model species, especially for mollusks for which very little related literature is available. Herein, we suggest an effective optical tissue clearing procedure for the freshwater snail *Biomphalaria glabrata*, known as the intermediate host of the human parasite *Schistosoma mansoni*. This clearing procedure involves solvents with a minimal toxicity, preserves the endogenous fluorescence of labeled parasites inside snail tissues and is compatible with an immunolabeling procedure

KEYWORDS

Clarity ; Blood fluke ; Mollusk ; Immunolabeling ; 3D imaging

1. Introduction

Tissue clearing is an ancient method first developed in the early 1900's by Werner Spalteholz [1] to describe the anatomy of human and animal tissues and organs. The principle of tissue clearing is based on the modification of the refractive index (RI) of the considered object (usually written *n*, defined by the ratio between celerity -speed of light in vacuum-written *c*, and phase velocity of light in the considered medium, written v_p). Tissue clearing typically involves the following three steps, namely sample fixation, permeabilization, and/or decolorization to reach an optimal RI: the optically cleared sample is then kept in a high-RI solvent (usually between 1.38 and 1.56 [2]). This principle allows for visualization of global structures inside of an organ, avoiding the deformation of information unfortunately inseparable from histological cuts. In line with the evolution of 3D imaging (multiphoton microscopy, light sheet microscopy) and image processing software (*e.g.* Imaris), several chemical transparency techniques were designed depending on the applications they were made for [2,3]. Thus, some protocols are more adapted to immunostaining while some other are compatible with the conservation of endogenous fluorescence [4]. For all clearing methods, one of the main challenges is dealing with the heterogeneity of the object to analyze, this heterogeneity could lead in light scattering through the different phases that the object may contain (each part of the object may react differently to the same treatments). Indeed, some clearing protocols are more effective at clearing certain organs for which some other are less efficient, in respect to the specific composition of such organs [5–7]. Especially regarding hemoglobin, its accumulation in tissues due to red blood cell lyses can reduce the efficiency of clearing procedure and increase autofluorescence [5,8]. The literature regarding non-optical clearing of non-model invertebrates is very limited [9–13], this is particularly true for mollusks [10,12,14] and especially in the context of parasitic infection [13]. *Biomphalaria glabrata* (Say, 1818) is the intermediate freshwater snail host of the trematode parasite *Schistosoma mansoni* (Sambo, 1907). This parasite can complete its life cycle through the infestation of a human definitive host, in which transmission occurs by direct skin contact with the fresh-water swimming larvae, called furcocercariae. Considered as a neglected tropical disease, schistosomiasis affects about 240 million people worldwide [15], affecting especially tropical and subtropical countries. However, since 2013, the disease has been considered established in Europe, specifically in France [16]. To achieve its life cycle, *S. mansoni* infests a definitive mammalian host in which the hematophagous parasite reaches its adult stage and sexually reproduces, laying eggs spread in the environment by host's feces. In contact with freshwater, eggs hatch and free ciliated miracidium larvae seeking for an intermediate snail host to infest from the genus *Biomphalaria*, such as snails from the species *B. glabrata* [17]. Following snail infection two scenarios can occur: either the host and the parasite are involved in a compatible interaction, in which the parasite exhibits a regular development, or, the host and the parasite are involved in an incompatible interaction resulting in the recognition, encapsulation and killing of the parasite by the snail's immune system [18–21]. *B. glabrata* is thus especially studied for its immune system and its link with this polymorphism of compatibility [22,23]. To improve the understanding of phenomena occurring following an infestation, histological approaches have been conducted on *Biomphalaria*, from the depiction of the parasite route within the snail [17], the description of capsules within snail tissues [24,25] to the recent unveiling of the histological atlas for *Biomphalaria* [26]. However, none of the previous methods applied for studying *Biomphalaria* tissues are designed for 3D-visualization of the planorbid snail. In this context, to study *Biomphalaria* 3D-organization at tissular and cellular levels, label proteins of interest and monitor parasite infestation inside the whole snail organism, we implemented an optical tissue clearing method adapted to this organism model.

Herein, we propose to enhance our understanding of the black box constituted by the interaction between the snail *B. glabrata* and its parasite *S. mansoni*, especially by deciphering the complex interaction between the parasite and the snail immune system. In this context, an efficient tissue clearing protocol would bring new perspectives for monitoring *S. mansoni* infestation in *B. glabrata* and would allow for a new visualization perspective of proteins inside the organism through immunolabeling. The present work details the method applied for *B. glabrata* whole individuals' tissue clearing and gives new research applications of this method in the context of *S. mansoni* infestation.

2. Method

2.1. Ethics statement

Our laboratory holds permit #39910–2022121915564694 (APAFIS number) for experiments on animals from both the French Ministry of Agriculture and Fisheries, and the French Ministry of National Education, Research, and Technology. The housing, breeding, and animal care of the utilized animals followed the ethical requirements of our country. The researchers also possess an official certificate for animal experimentation from both French ministries (Decree # 87–848, October 19, 1987). Animal experimentation followed the guidelines of the French CNRS. The different protocols used in this study had been approved by the French veterinary agency from the DDPP Languedoc-Roussillon (Direction Departementale´ de Protection des Populations), Montpellier, France (authorization # 007083) and the Ethic committee CEEALR (#C66-136-01).

2.2. Biological material, parasite recovery and infestation

Golden hamsters (*Mesocricetus auratus*) were infested with 700 cercariae of *S. mansoni* Puerto Rican NMRI strain. Seven weeks postinfection, hamsters' livers were recovered and ground in saline solution (150 mM NaCl), parasite's eggs contained in the liver extract were then recovered by filtration through sieves (with a final mesh size of 45 µm).
Eggs were hatched in fresh water and miracidia were manually collected by pipetting and transferred to a 1.5 mL Eppendorf tube for downstream analysis. Miracidia were stained for 30 min with a green, fluorescent CellTracker™ probe: 5-chloromethylfluorescein diacetate, CMFDA (ref. C7025, ThermoFisher) as previously described [27]. *B. glabrata* snails from the albino BgBRE2 strains (Recife, Brazil), and melanized BS-90 strain (Salvadore, Brazil) [28] were exposed to stained miracidia for 24h before being proceeded for clearing procedure.

2.3. Clearing procedure

Clearing procedure was performed using X-CLARITY™ system (Polymerization System and Clearing System II) located at network facilities RHEM-Biocampus in Montpellier. The whole procedure was carried out through three steps: sample fixation, hydrogel inclusion and delipidation. Briefly, *B. glabrata* individuals' shells were removed and snails were fixed for 24h in 4 % paraformaldehyde at 4 °C. The snails used had a diameter range of 6 mm–11 mm, corresponding to a weight range of 40 mg–90 mg (without the shell and before fixation). Regarding infested snails, fixation was done 24h after exposure to the parasite. Fixed snails were washed 3 times in Phosphate Buffered Saline solution (PBS), then they were incubated in hydrogel (from logosBiosystems: 4 % *v/v* Acrylamide, 0.25 % *m/v* VA-044, in PBS, no aldehydes were added in the hydrogel solution) for acrylamide passive penetration during 24h at 4 °C. Samples were then stand in hydrogel for 3h at 37 °C under vacuum for acrylamide polymerization. Finally, they are rinsed in PBS solution for 24h at 4 °C before proceeding to the clearing step as such (at that stage we can leave the specimens at 4 °C for a week). Clearing by lipids removal is performed actively through electrophoresis for 120h, before performing a passive step for 48h at 37 °C, both steps (active and passive) use the same clearing solution composition (200 mM boric acid, 4 % *m/v* SDS detergent, pH 8.5). Samples were washed for 24h at 37 °C with PBS solution. Cleared samples are put until used in a mix solution of 80 % glycerol in PBS adjusted to a RI of 1.46 nD using a refractometer (Mettler Toledo, 30PX refractometer model). The refractometer's light source emits at 589,3 nm and the measurement was taken at 20 °C.

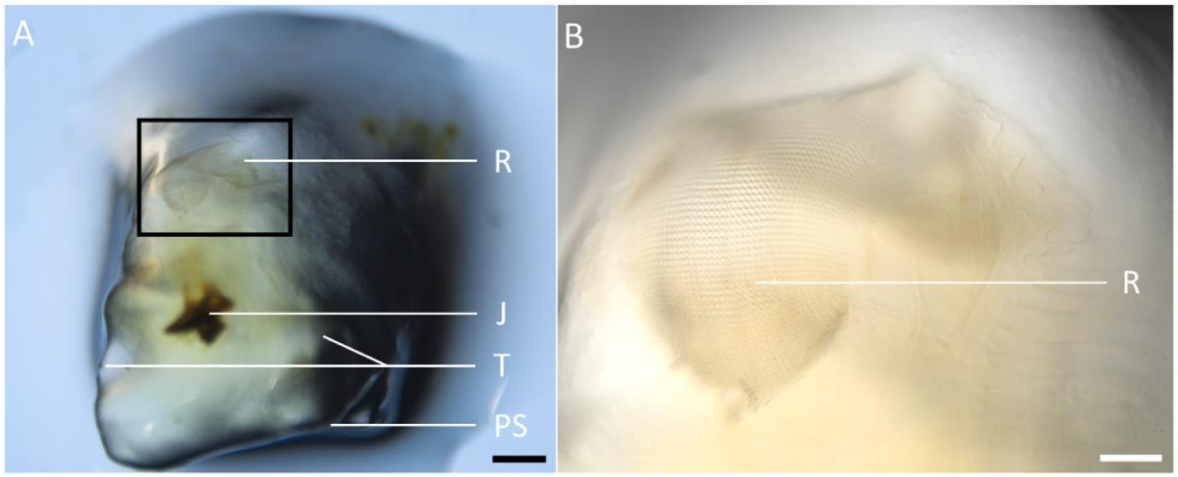

Fig. 1. Front part of *B. glabrata* snail after tissue clearing (A) and magnification of the black-framed area containing the radula of the same individual (B). This part of the snail is fully cleared, only letting chitin-containing parts uncleared. J: Jaws, PS: Pedal Sole, R: Radula, T: Tentacle area. Scale bars:1000 µm (A) and 150 µm (B). An uncleared full specimen can be seen in Appendix A for information.

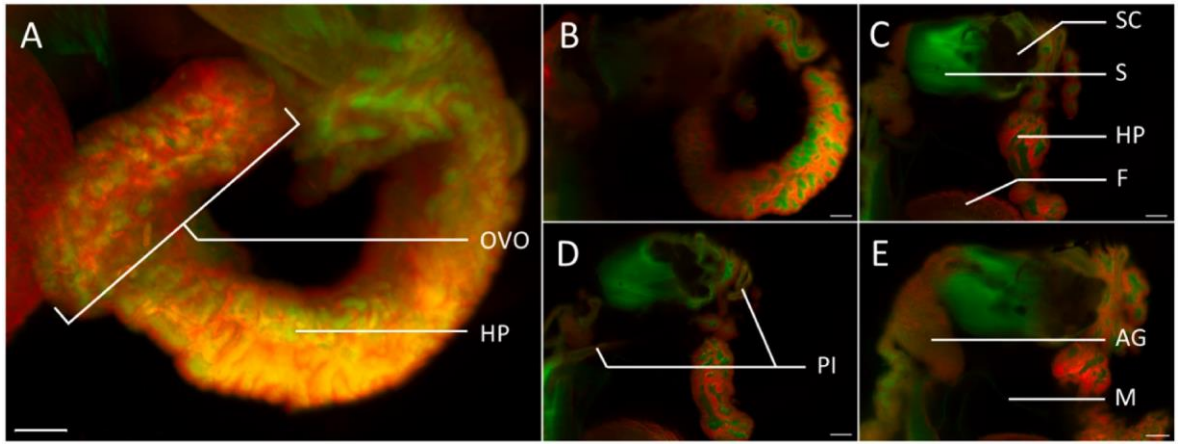

Fig. 2. Optically cleared visceral mass from an individual of *B. glabrata* observed in light sheet microscopy. A: 3D reconstruction of the hepatopancreas area after a serial acquisition, B, C, D, E: four focal planes taken in the thickness of the same individual. In B, green autofluorescence of the hepatopancreas is remarkable inside of each lobe, C and D planes show stomach with a high green autofluorescence and intestine while in E the albumen gland is clearly noticeable. AG: Albumen Gland, F: Foot, HP: Hepatopancreas, M: Mantle, OVO: Ovotestis, PI: Posterior part of the Intestine, S: Stomach, SC: Stomach Cavity. Red: propidium iodide, green: tissular autofluorescence. Scale bars: 200 µm. Dynamic 3D representation of a snail is available in Appendix B. An uncleared full specimen is shown in Appendix A, permitting the assessment of organ location in the snail.

2.4. Immunolabeling and nuclei staining

Samples were immunostained with an anti-Biomphalysin 1 antibody. It was designed using a peptide (INALDRNDVNWADDA) injected into a rabbit. Purification from the rabbit serum was performed on a peptidecoupled affinity column.

Primary antibody staining was performed for 5 days at 37 °C in a solution of 1 % (v/v) Triton X-100. Samples are washed for 24h at 37 °C in a solution of 0.1 % Triton X-100 in PBS. Fluorescent labeling was performed using an Invitrogen Alexa Fluor 488 anti-rabbit antibody (ThermoFisher, A-21206). Thereafter, specimens are washed in 0.1 % Triton X-100 PBS for 24h at 37 °C. Nuclei were labeled using propidium iodide and samples were put in an 80 % glycerol solution diluted in PBS to reach a RI of 1.46, adjusted using a refractometer. Negative control condition was carried out using pre-immune serum from the same rabbit used for antibody production. Two snails were used for the control condition, and the same incubation time, temperature and buffers were used as the immunolabeled condition.

Imaging was performed using a light sheet imaging UltraMicroscope Blaze (Miltenyi Biotec) holding a 2 × MVPLAPO Olympus objective with a numerical aperture of 0.5 (acquisition step of 3 µm). The imaging medium was a glycerol solution with a RI of 1.46. We used 561 nm laser and a 620/60 filter for propidium iodide imaging and a 488 nm laser and a 525/50 filter for green fluorescence detection. Z stacks were performed according to the thickness of the light sheet. Confocal imaging was performed on a Zeiss LSM 700 microscope (Bioenvironment platform, University of Perpignan, France). Pictures were treated through Imaris software for light sheet captures and with Zen (Zeiss) software and ImageJ for confocal microscopy acquisitions. Pictures taken in white light in order to illustrate the efficiency of clearing procedure (including those included in graphical abstract), were performed using a Nikon SMZ18 stereomicroscope, using a Nikon DS-Fi3 camera and NISElements Imaging Software (Nikon).

3. Results

B. glabrata cleared specimens were used to check their global tissular organization through green autofluorescence and nuclei staining by using propidium iodide, simultaneously we assayed the conservation of endogenous green fluorescence brought by stained miracidia of *S. mansoni* used to infect the snails before clearing. *B. glabrata* organism is not able to initiate melanization following an infection or an injury, this pathway being incomplete for this species [29,30]. Thus this particularity allowed to avoid some issues often encounters in other invertebrate models due to this immune mechanism [11]. Nevertheless, if *Biomphalaria* snails were not able to melanize intruders during an immune response, they can exhibit different levels of melanization of their tissues, this is why the clearing procedure was

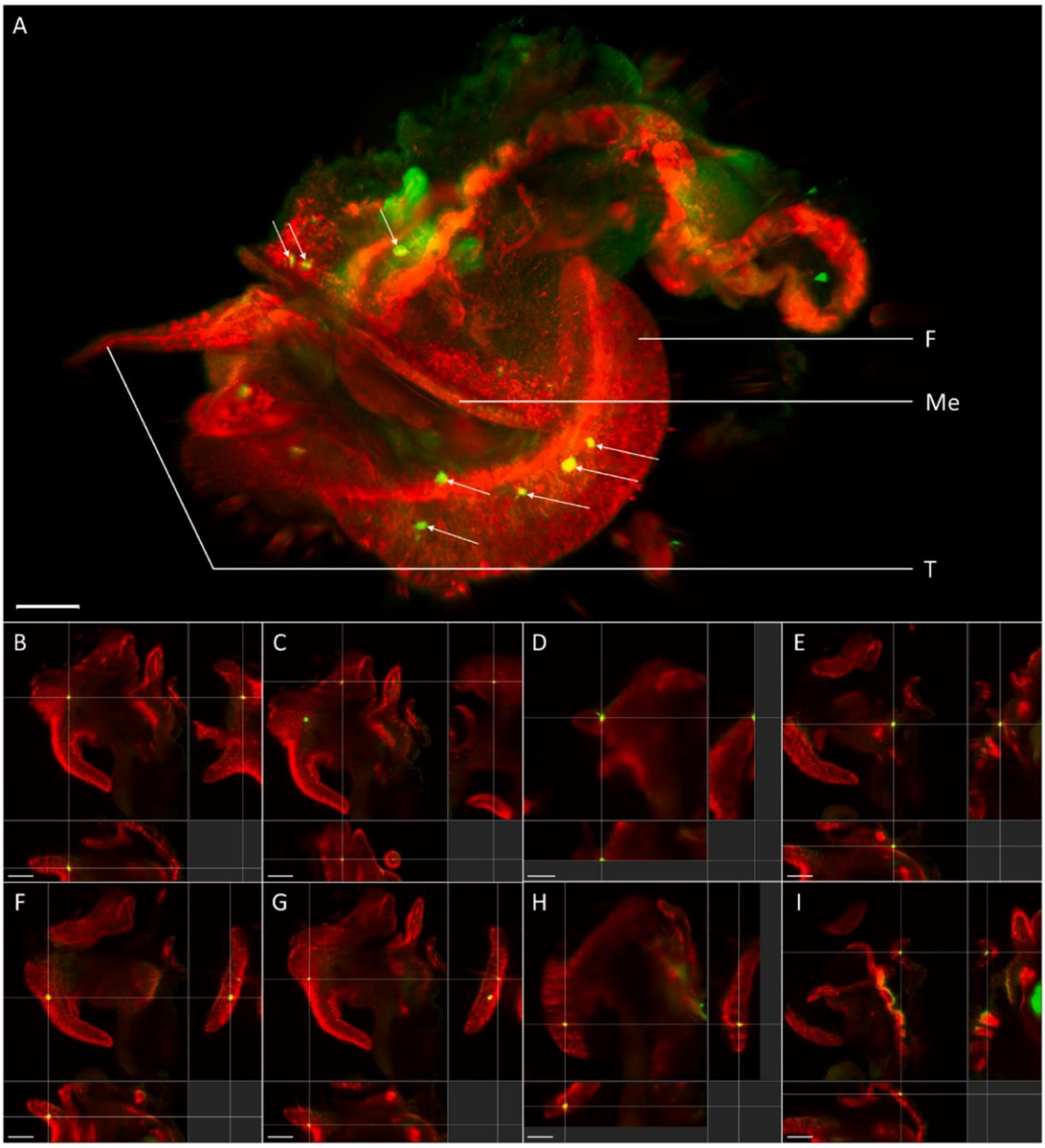

Fig. 3. Optically cleared snail of *B. glabrata* from albino BgBRE2 strain infested by *S. mansoni* NMRI strain miracidia observed in light sheet microscopy. Miracidia of *S. mansoni* transform close to their penetration site, *i. e.* the foot, the mantle edge and the pallial cavity [17,26]. A: Lateral view of the snail, some mother sporocysts are identified on the left side of the individual with white arrows. B to I: some parasites are shown through the orthogonal splicing of the host, giving their precise location within the infested snail, and making them easily distinguishable from background fluorescence or potential external artefacts. In B, D, F, G and H, sporocysts are found in the foot, in C, sporocyst is found in the cephalic region, in E, sporocyst is found in the roof of pallial cavity and in I, sporocyst has implanted in mantle edge of the snail. All nine pictures were captured from the same individual. Labels: F: Foot, Me: Mantle edge, T: Tentacle. Red: propidium iodide, green: CMFDA labeled parasites and snail autofluorescence. Scale bars: 300 µm. Dynamic 3D representation of another *B. glabrata* individual is available in Appendix B.

herein carried out on both an albino strain (BgBRE2) and a melanic strain (BS-90) of *B. glabrata* in order to assess the efficiency of the chosen procedure with the whole potential strain panel that could be used for further experimental approaches, as several studied strains of *B. glabrata* are melanic.

We succeeded to validate albino and melanized snails clearing through CLARITY method, only letting radula and jaws uncleared (Fig. 1A and B). In addition, black areas of the tegument of the melanized strain were perfectly cleared.

Tissue clearing coupled to propidium iodide staining allows for nuclei visualization, making the whole snail organization and their different organs visible. Main organs are quite easily recognizable, such as hepatopancreas, intestine and albumen gland, foot (Fig. 2), and radula for which autofluorescence is particularly strong, as previously documented [31,32]. Tissues exhibited different autofluorescence levels for the green channel, some tissues with a high green auto-fluorescence as for examples the stomach due to its strong density and the hepatopancreas (noticeable even in a single plane as shown in Fig. 2) while this autofluorescence was far lower using the red channel (Appendix B).

As performed previously, fluorescently stained miracidia larvae were prepared for snail infestations [27]. This procedure allows here to assay the conservation of endogenous fluorescence after clearing. Mother sporocysts usually start to develop closely to the miracidium penetration site [17]. In the context of infested snails, green-labeled parasites can be easily observed and their position and interactions within the snail may then be

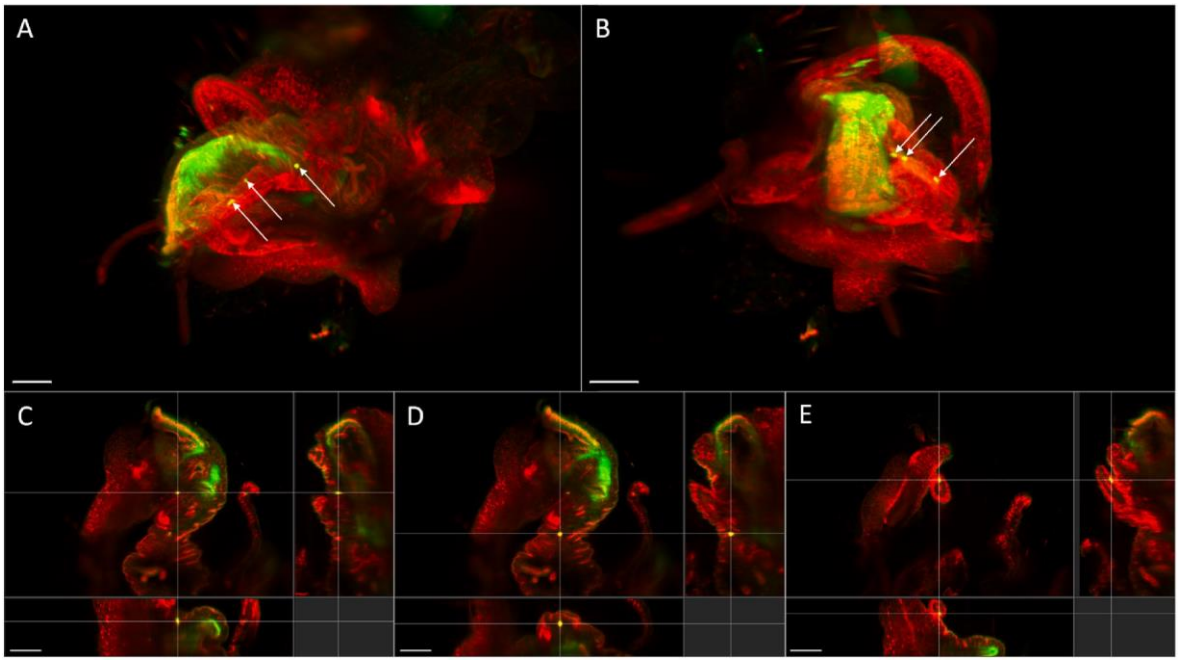

Fig. 4. Optically cleared snail of *B. glabrata* from the melanized BS-90 strain infested by *S. mansoni* NMRI strain miracidia. A, B: Lateral and front views of the snail, radula autofluorescence is remarkable, three mother sporocysts are noticed on the left side of the individual (white arrows). Those parasites are identified through the orthogonal splicing of the host, taken at different Z-value in C, D and E, giving their precise location within the infested snail tissues, making them easily distinguishable from background fluorescence. All five pictures were taken from the same individual. Red: propidium iodide, green: CMFDA labeled parasites and snail autofluorescence. Scale bars: 300 µm.

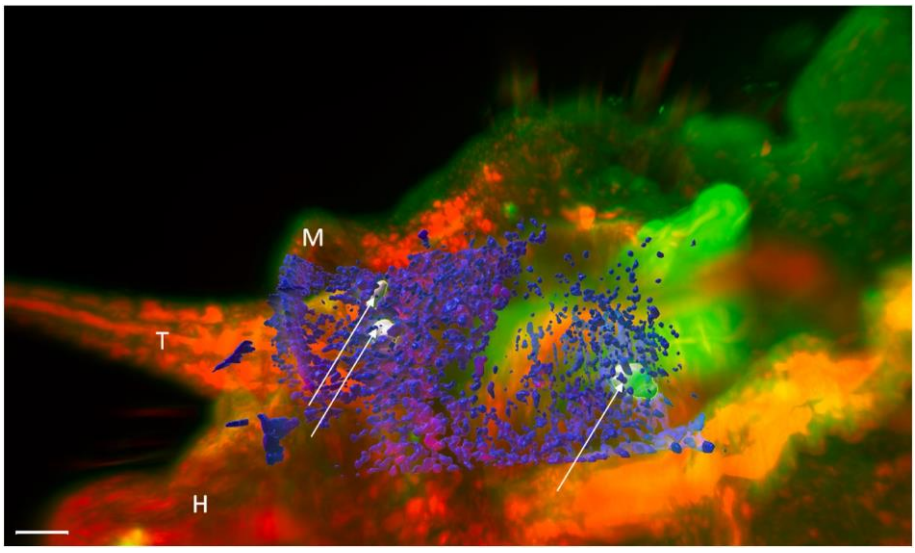

Fig. 5. Light sheet microscopy visualization of a BgBRE2 strain snail infested by *S. mansoni* NMRI sporocysts. Surface constructions provide a better spatial rendering of the position of sporocysts. Surfaces of three sporocysts are defined in the foreground in white (indicated by white arrows) while snail tissue surfaces corresponding to nucleic staining are colored in blue. H: Head, M: Mantle edge, T: Tentacle. More details are given through a 3D dynamic representation in Appendix C.

depicted (Figs. 3 and 4). Orthogonal views are especially presented to show deepness penetration of fluorescent parasites in the three dimensions within snail tissues (Fig. 3B–I and Fig. 4C–E). As an example, sporocysts may sometime develop near or directly on tentacles of snails as shown in Fig. 4E.

Autofluorescence in the green channel is highly visible but still below fluorescence intensity level of parasites especially looking at the orthogonal views (corresponding to one focal slice), on which labeling intensity is noticeably superior to background fluorescence (Figs. 3 and 4).

Even if orthogonal views allowed for a clear positioning of parasites, their relative position within the host can be monitored directly using 3D visualization through the surface plotting of fluorescent structures (Fig. 5). Sporocysts flushing snail tissues can be easily identified based on host's nucleic surfaces observed around the miracidium penetration site (Fig. 5).

Optical acquisition can be performed using confocal microscopy, even for some large specimens, enabling areas of interest to be explored in detail, since the defined zones are flush with or close to the surface of the object (Figs. 5 and 6). This type of acquisition allows for far more detailed biological observations such as interactions in-between parasites or between parasites and host's cells. Our results demonstrated that tissue clearing allows for a deeper visualization in tissues compared to histological cuts, including vibratome thick cuts.

Immunolabeling is compatible with CLARITY clearing method (Fig. 7), allowing for time gaining immunolocalization of structures of interest. Here are exhibited immunolabeling for a humoral factor involved in killing parasite [33,34] present in the foot (Fig. 7 A) and in the mantle edge of the snail (Fig. 7 B). 3D reconstruction of the sample following Z-stack imaging allows for a clear visualization of labeled tissues inside the whole snail organism and even

displays the biological shape of labeled tissues or organs. As the whole snail tissues are transparent after treatment, sample thickness constitutes the main parameter that may reduce fluorescence recording, specifically regarding potential autofluorescence, if labeled structures are very small or labeling intensity is low. Also, in some cases immunolabeling may be preferably performed only on subsections of the snails to focus on regions of interest.

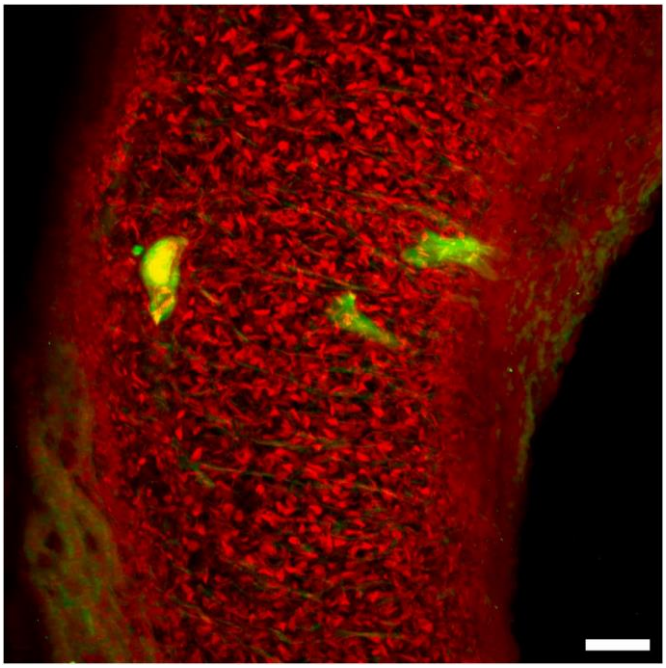

Fig. 6. Confocal microscopy acquisition of NMRI strain sporocysts within the BgBRE2 strain snail. Acquisition was performed on a deepness of approximately 2500 µm. Those pictures were taken to the deepest attainable limit within the snail. The present picture corresponds to the Z-stack of the 70 pictures acquired (140 including both channels). Red: propidium iodide, green: CMFDA labeled parasites. Scale bar: 50 µm. A 3D visualization of those focal plane acquisitions is accessible in Appendix D.

4. Discussion

Optical clearing through X-CLARITY procedure allowed for a good transparency of the whole *B. glabrata* organism and tissues. This procedure is effective for albino strains of *B. glabrata* as well as for the melanized BS-90 strain. In the context of a work on *B. glabrata*-parasite interaction, this procedure may be of interest for co-infection studies, allowing to follow several parasites stained with different labels, helping in the understanding of their dynamics and potential interactions within the host snail. This procedure may be particularly relevant for monitoring a sequential infestation as for example to study innate immune memory in *B. glabrata* snails, and allowing to distinguish first and second
S. mansoni parasite infestation, using fluorophores with different emission wavelengths for parasite labeling [35,36]. Moreover, contrary to more conventional methods yet developed to monitor parasite infestation, tissue clearing may permit to exhaustively follow the *Schistosoma* infestation status without altering the whole snail structure (either by dissection or by histological cutting). This method may allow subsequently works on the same individual, for which the infestation status and parasite intensity may thus be determined. Those subsequent studies may include an expression monitoring for candidate genes by RNAscope or a protein study by immunolabeling of host's immune humoral compounds, cellular proteins [19,34,37,38] or parasite secretory products [39].

We showed that this tissue clearing procedure can be compatible also with immunolabeling, avoiding in some circumstances the use of microtome, or providing support to more classical histology procedures. However, the described procedure may be inadequate for immunolabeling of some membranous or hydrophobic compounds since this method contains an electrophoretic delipidation step of the samples, which may discard some molecules of interest depending on the experimental project considered. The targeted molecule selected to exhibit immunolabeling compatibility is known to be a soluble immune protein [34], however seen to be found inside of membranous structures (Fig. 6).

This optical clearing method has the great advantage to avoid the use of toxic solvents and hazardous buffer preparation (which is the case for DISCO procedure and its derivatives, for example, through the use of benzoyl benzoate [2]), moreover, once made cleared, samples can be stored for several weeks in glycerol after immunolabeling, provided they are kept in the dark. X-Clarity has also the advantage to be conducted on a short time using an active electrophoresis, comparing to some other procedures for which a longer time can be required to fully achieve clearing [2]. Sample visualization is an important step especially as 3D microscopy has undergone significant development particularly with high resolution optical sectioning microscopies that allow for cellular level acquisitions in big samples [40]. As it can be noticed from tissue fluorescent labeling throughout the presented results, a strong tissue-specific green auto-fluorescence is exhibited. This autofluorescence may potentially interfere with some signal visualization, especially regarding hepatopancreas, stomach and radula (Figs. 2 and 3). However, this autofluorescence being specifically strong in the green channel, the use of a compatible fluorochrome with a proper emission wavelength must be done to diminish or avoid this green autofluorescence depending on the snail area monitored. Focal plans orthogonal observation still enables autofluorescent

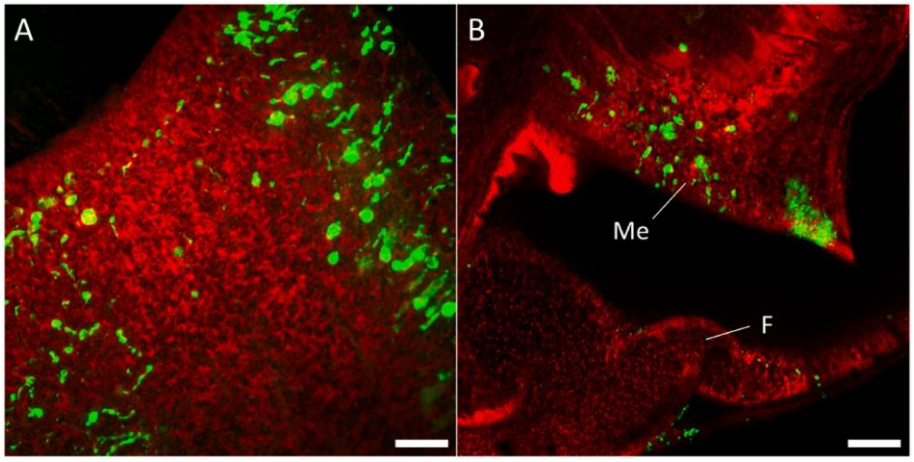

Fig. 7. Confocal visualization of Biomphalysin immunolabeling for BgBRE2 strain snail. A: Z-stack of the foot of BgBRE2 individual immunolabeled, B: Focal plane showing the mantle edge (Me) and a part of the foot of an individual (F). Red: propidium iodide, green: immunolabeling of Biomphalysin 1. Scale bars: 150 µm. More details can be seen in Appendix E and F. Negative control can be seen in Appendix G, incubated with pre-immune serum.

tissues to be separated from the relevant signal and the selection of areas of interest permits to avoid the impact of a given autofluorescent tissue.

Herein, the depicted results were captured either using macro-light sheet and confocal microscope. Thus, a deeper sample visualization could be performed using clarity dedicated objectives for light sheet microscope to reach cellular levels with a better resolution. Quality and integrity of biological structures was preserved after clearing, as well as endogenous fluorescence of the parasites which was still detectable several weeks after treatment. Finally, we must be careful that samples are kept in glycerol with a homogenous RI to avoid sample dehydration, and that the picture acquisitions are taken in conditions avoiding dehydration of the studied samples. The depicted clearing method is compatible with albino strains of *B. glabrata* but also with melanized individuals [18], making it possible to exhaustively monitor the parasite count within the snail intermediate host regardless of the studied snail strain. It will thus be possible to study the strain-specific relationship between *B. glabrata* snails and *S. mansoni* parasites through *in situ* monitoring of the key factors involved in parasite survival or killing within the snail, either by RNA or protein-based methods.

Funding

The author(s) declare financial support was received for the research work. The funders had no role in study design, data collection and analysis, decision to publish, or preparation of the manuscript. DD, PP and BG were supported by the ANR AEROSNAIL (ANR-19-CE11-001601) from the French National Research Agency (ANR). RHEM facility was supported by SIRIC Montpellier Cancer (Grant INCa_Inserm_DGOS_12553), the European regional development foundation and the Occitanie region (FEDER-FSE 2014–2020 Languedoc Roussillon). The imaging facility MRI was supported by the French National Research Agency (ANR-10-INBS-04, «Investments for the future»).

CRediT authorship contribution statement

Pierre Poteaux: Conceptualization, Methodology, Validation, Investigation, Resources, Data curation, Writing – original draft, Writing – review & editing, Visualization, Project administration. **Chantal Ripoll:** Methodology, Investigation, Resources, Writing – review & editing. **Amelie´ Sarrazin:** Methodology, Investigation, Resources, Writing – review & editing, Visualization. **Marie-Pierre Blanchard:** Methodology, Investigation, Resources. **Anne Guillou-Duvoid:** Conceptualization. **BenjaminGourbal:** Writing – original draft, Writing – review & editing. **Hel´ ene Hirbec:`** Funding acquisition. **David Duval:** Conceptualization, Methodology, Writing – original draft, Writing – review & editing, Supervision, Funding acquisition.

Declaration of competing interest

The authors declare that they have no known competing financial interests or personal relationships that could have appeared to influence the work reported in this paper.

Data availability

Data will be made available on request.

Acknowledgements

The authors want to thank the technical staff of the IHPE laboratory, Anne Rognon, Damien Pouzol and Olivier Portela for the maintenance of mollusk strains and their expertise on animal experimentation. We are grateful to Paradev Compagny for having facilitated the parasite egg collection. We acknowledge the "Reseau d´ 'Histologie Exp´erimentale de Montpellier" - RHEM facility supported by SIRIC Montpellier Cancer (Grant INCa_Inserm_DGOS_12553), the European regional development foundation and the Occitanie region (FEDER-FSE 2014–2020 Languedoc Roussillon). We acknowledge the imaging facility MRI, member of the France-BioImaging national infrastructure supported by the French National Research Agency (ANR-10-INBS-04, «Investments for the future») for image acquisitions. This study is set within the framework of the "Laboratoires d'Excellences (LABEX)" TULIP (ANR-10-LABX-41) and CeMEB (ANR-10-LABX-04-01).

Appendix A. Supplementary data

Supplementary data to this article can be found online at https://doi.org/10.1016/j.fsi.2024.109800.

References

[1] W. Spalteholz, Über das Durchsichtigmachen von menschlichen und tierischen Praparaten¨ : nebst Anhang, Über Knochenfarbung¨ , Leipzig: Verlag von S. Hirzel (1911).

[2] D.S. Richardson, J.W. Lichtman, Clarifying tissue clearing, Cell 162 (2) (Jul. 2015) 246–257, https://doi.org/10.1016/j.cell.2015.06.067.

[3] M. Muntifering, D. Castranova, G.A. Gibson, E. Meyer, M. Kofron, A.M. Watson, Clearing for deep tissue imaging, Curr Protoc Cytom 86 (1) (Oct. 2018) e38, https://doi.org/10.1002/cpcy.38.

[4] I.P. Pavlova, S.C. Shipley, M. Lanio, R. Hen, C.A. Denny, Optimization of immunolabeling and clearing techniques for indelibly-labeled memory traces, Hippocampus 28 (7) (Jul. 2018) 523–535, https://doi.org/10.1002/hipo.22951.

[5] H. Kolesova,´ V. Olejní˘ckova,´ A. Kvasilova,´ M. Gregorovi˘cov´a, D. Sedmera, Tissue clearing and imaging methods for cardiovascular development, iScience 24 (4) (Apr. 2021) 102387, https://doi.org/10.1016/j.isci.2021.102387.

[6] J. Xu, Y. Ma, T. Yu, D. Zhu, Quantitative assessment of optical clearing methods in various intact mouse organs, J. Biophot. 12 (2) (2019) e201800134, https://doi.org/10.1002/jbio.201800134.

[7] Y.-J. Zhan, S.-W. Zhang, S. Zhu, N. Jiang, Tissue clearing and its application in the musculoskeletal system, ACS Omega 8 (2) (Jan. 2023) 1739–1758, https://doi.org/10.1021/acsomega.2c05180.

[8] K. Sung, et al., Simplified three-dimensional tissue clearing and incorporation of colorimetric phenotyping, Sci. Rep. 6 (1) (Aug. 2016), https://doi.org/10.1038/ srep30736, 1.

[9] A. Konno, S. Okazaki, Aqueous-based tissue clearing in crustaceans, Zoological Letters 4 (1) (Jun. 2018) 13, https://doi.org/10.1186/s40851-018-0099-6.

[10] V.A. Milichko, V. Dyachuk, 3D optical reconstruction of the nervous system of the whole-body marine invertebrates, Chemical & Biomedical Imaging 1 (9) (Dec. 2023) 852–863, https://doi.org/10.1021/cbmi.3c00087.

[11] L. Moya-Anderico,´ J. Admella, E. Torrents, A clearing protocol for Galleria mellonella larvae: visualization of internalized fluorescent nanoparticles, N. Biotech. 60 (Jan. 2021) 20–26, https://doi.org/10.1016/j.nbt.2020.08.002.

[12] M. Pende, et al., A versatile depigmentation, clearing, and labeling method for exploring nervous system diversity, Sci. Adv. 6 (22) (May 2020) eaba0365, https://doi.org/10.1126/sciadv.aba0365.

[13] S. Schuster, et al., Developmental adaptations of trypanosome motility to the tsetse fly host environments unravel a multifaceted in vivo microswimmer system, Elife 6 (Aug. 2017) e27656, https://doi.org/10.7554/eLife.27656.

[14] A.A. Petrov, E.V. Soldatenko, A simple and low-cost method to visualize musculature and other aspects of anatomy by confocal microscopy, Microsc. Res. Tech. 86 (5) (2023) 565–572, https://doi.org/10.1002/jemt.24295.

[15] WHO, Ending the Neglect to Attain the Sustainable Development Goals: A Road Map for Neglected Tropical Diseases 2021–2030, vol. 63, World Health Organization, Geneva, 2020 [Online]. Available: https://www.who.int/publicat ions-detail-redirect/9789240010352. (Accessed 9 January 2024).

[16] A. Berry, et al., "Evidence for a permanent presence of schistosomiasis in Corsica, France, 2015,", Euro Surveill. 21 (1) (Jan. 2016) https://doi.org/10.2807/15607917.ES.2016.21.1.30100, 1.

[17] E.T. Abdel-Malek, Anatomy of Biomphalaria boissyi as related to its infection with schistosoma mansoni, Am. Midl. Nat. 54 (2) (1955), https://doi.org/10.2307/ 2422574, 2.

[18] R. Galinier, et al., A multistrain approach to studying the mechanisms underlying compatibility in the interaction between Biomphalaria glabrata and Schistosoma mansoni, PLoS Neglected Trop. Dis. 11 (3) (Mar. 2017), https://doi.org/10.1371/journal.pntd.0005398, 3.

[19] H. Li, et al., Coordination of humoral immune factors dictates compatibility between Schistosoma mansoni and Biomphalaria glabrata, Elife 9 (2020), https://doi.org/10.7554/eLife.51708.

[20] G. Mitta, B. Gourbal, C. Grunau, M. Knight, J.M. Bridger, A. Theron, Chapter three -´ the compatibility between Biomphalaria glabrata snails and schistosoma mansoni: an increasingly complex puzzle, in: D. Rollinson, J.R. Stothard (Eds.), Advances in Parasitology, vol. 97, Academic Press, 2017, pp. 111–145, https://doi.org/10.1016/bs.apar.2016.08.006.

[21] T.P. Yoshino, B. Gourbal, A. Th´eron, Schistosoma Sporocysts, 2016, p. 31.

[22] P.C. Hanington, M.A. Forys, E.S. Loker, A somatically diversified defense factor, FREP3, is a determinant of snail resistance to schistosome infection, PLoS Neglected Trop. Dis. 6 (3) (Mar. 2012), https://doi.org/10.1371/journal. pntd.0001591, 3.

[23] A. Portet, et al., Integrated multi-omic analyses in Biomphalaria-Schistosoma dialogue reveal the immunobiological significance of FREP-SmPoMuc interaction, Dev. Comp. Immunol. 75 (Oct. 2017) 16–27, https://doi.org/10.1016/j.dci.2017.02.025.

[24] E.S. Loker, C.J. Bayne, P.M. Buckley, K.T. Kruse, Ultrastructure of encapsulation of schistosoma mansoni mother sporocysts by hemocytes of juveniles of the 10-R2 strain of Biomphalaria glabrata, J. Parasitol. 68 (1) (1982) 84–94, https://doi.org/10.2307/3281328.

[25] J.T. Sullivan, C.S. Richards, Schistosoma mansoni, NIH-SM-PR-2 strain, in susceptible and nonsusceptible stocks of Biomphalaria glabrata: comparative histology, J. Parasitol. 67 (5) (1981) 702–708, https://doi.org/10.2307/3280445.

[26] Z. de Araújo Andrade, S. Souza Svigel, M.J. Faro, Atlas de histologia de Biomphalaria glabrata, Editora CRV, 2022, https://doi.org/10.24824/ 978652512904.4.

[27] D. Duval, P. Poteaux, B. Gourbal, A. Rognon, R.D.C. Augusto, Fluorescent non transgenic schistosoma to decipher host-parasite phenotype compatibility, Front. Immunol. 14 (2023). Accessed: Dec. 17, 2023. [Online]. Available: https://www.frontiersin.org/articles/10.3389/fimmu.2023.1293009.

[28] W.L. Paraense, L.R. Correa, Variation in susceptibility of populations of Australorbis glabratus to a strain of Schistosoma mansoni, Rev. Inst. Med. Trop. Sao Paulo 5 (1963) 15–22.

[29] E.S. de Melo, F.A. Brayner, N.C.P. Junior, I.R.S. França, L.C. Alves, Investigation of defense response and immune priming in Biomphalaria glabrata and Biomphalaria straminea, two species with different susceptibility to Schistosoma mansoni, Parasitol. Res. 119 (1) (Jan. 2020) 189–201, https://doi.org/10.1007/s00436-01906495-4.

[30] W. Le Clec'h, T.J.C. Anderson, F.D. Chevalier, Characterization of hemolymph phenoloxidase activity in two Biomphalaria snail species and impact of Schistosoma mansoni infection, Parasites Vectors 9 (Jan. 2016) 32, https://doi. org/10.1186/s13071-016-1319-6.

[31] J.T. Haug, et al., Autofluorescence imaging, an excellent tool for comparative morphology, J. Microsc. 244 (3) (2011) 259–272, https://doi.org/10.1111/j.13652818.2011.03534.x.

[32] W. Krings, C. Neumann, S.N. Gorb, A. Koehnsen, H. Wagele,¨ Elemental composition and material properties of radular teeth in the heterobranch snail Gastropteron rubrum (Mollusca, Gastropoda, Cephalaspidea) foraging on hard organisms, Ecol. Evol. 13 (8) (Aug. 2023) e10332, https://doi.org/10.1002/ ece3.10332.

[33] R. Galinier, et al., Biomphalysin, a new β pore-forming toxin involved in Biomphalaria glabrata immune defense against schistosoma mansoni, PLoS Pathog. 9 (3) (Mar. 2013), https://doi.org/10.1371/journal.ppat.1003216, 3.

[34] S. Pinaud, et al., New insights into Biomphalysin gene family diversification in the vector snail Biomphalaria glabrata, Front. Immunol. 12 (Apr) (2021), https://doi.org/10.3389/fimmu.2021.635131.

[35] S. Pinaud, et al., Molecular characterisation of immunological memory following homologous or heterologous challenges in the schistosomiasis vector snail, Biomphalaria glabrata, Dev. Comp. Immunol. 92 (Mar. 2019) 238–252, https://doi.org/10.1016/j.dci.2018.12.001.

[36] S. Pinaud, et al., A shift from cellular to humoral responses contributes to innate immune memory in the vector snail Biomphalaria glabrata, PLoS Pathog. 12 (1) (Jan. 2016), https://doi.org/10.1371/journal.ppat.1005361, 1.

[37] E.A. Pila, M. Tarrabain, A.L. Kabore, P.C. Hanington, A novel toll-like receptor (TLR) influences compatibility between the gastropod Biomphalaria glabrata, and the digenean trematode schistosoma mansoni, PLoS Pathog. 12 (3) (Mar. 2016) e1005513, https://doi.org/10.1371/journal.ppat.1005513.

[38] R. Pichon, et al., Single cell RNA sequencing reveals hemocyte heterogeneity in Biomphalaria glabrata: plasticity over diversity, Front. Immunol. 13 (Sep. 2022) 956871, https://doi.org/10.3389/fimmu.2022.956871.

[39] F. Guillou, et al., Excretory–secretory proteome of larval Schistosoma mansoni and Echinostoma caproni, two parasites of Biomphalaria glabrata, Mol. Biochem. Parasitol. 155 (1) (Sep. 2007), https://doi.org/10.1016/j. molbiopara.2007.05.009, 1.

[40] J. Zhao, H.M. Lai, Y. Qi, D. He, H. Sun, Current status of tissue clearing and the path forward in neuroscience, ACS Chem. Neurosci. 12 (1) (Jan. 2021) 5–29, https://doi.org/10.1021/acschemneuro.0c00563.